Two tryptophans are better than one in accelerating electron flow through a protein

Kana Takematsu,[a] Heather Williamson,[b] Pavle Nikolovski,[c] Jens T. Kaiser,[c] Yuling Sheng,[c] Petr Pospíšil,[d] Michael Towrie,[e] Jan Heyda,[d,f] Daniel Hollas,[f] Stanislav Záliš,[d,*] Harry B. Gray,[c,*] Antonín Vlček,[d,g,*] and Jay R. Winkler[c,*]

[a] Department of Chemistry, Bowdoin College, Brunswick, ME 04011, USA
[b] Department of Chemistry, Xavier University of Louisiana, New Orleans, LA 70125, USA
[c] Beckman Institute, California Institute of Technology, Pasadena, CA 91125, USA
[d] J. Heyrovský Institute of Physical Chemistry, Academy of Sciences of the Czech Republic, Dolejškova 3, CZ-182 23 Prague, Czech Republic
[e] Central Laser Facility, Research Complex at Harwell, Science and Technology Facilities Council, Rutherford Appleton Laboratory, Harwell Oxford, Didcot, Oxfordshire, OX11 0FA, UK
[f] Department of Physical Chemistry, University of Chemistry and Technology, Prague, Technická 5, CZ-166 28 Prague, Czech Republic
[g] Queen Mary University of London, School of Biological and Chemical Sciences, Mile End Road, London E1 4NS, United Kingdom

*E-mails: winklerj@caltech.edu; avlcek@qmul.ac.uk; hbgray@caltech.edu; zalis@jh-inst.cas.cz

Supporting Information

Table of contents:

Section S1: Crystal structures

Table S1. X-ray data collection, refinement statistics, and validation for Re-labeled azurins. Data for outermost shells are given in parentheses.

	ReH126W124W122Cu^{II}	**ReH126W124F122Cu^{II}**	**ReH126F124W122Cu^{II}**
X-ray data collection	SSRL beamline 12-2	In-house rotating anode	In-house rotating anode
Wavelength (Å)	1.0000	1.5418	1.5418
Unit cell (Å)	53.072, 221.563, 89.996	97.91, 33.97, 77.26	62.25, 62.26, 133.69
Space group	$C222_1$	C121	$P2_12_12_1$
Resolution range (Å)	35.00-1.85 (1.95-1.85)	38.4-1.9 (2.0-1.9)	45.95-2.0 (2.06-2.01)
Unique reflections (#)	44003 (6369)	19028 (2625)	34806 (2493)
Multiplicity	3.3 (3.4)	2.4 (2.5)	2.8 (2.6)
Completeness (%)	96.2 (96.3)	93.8 (88.8)	97.6 (96.2)
<I/σ(I)>	8.3 (1.4)	9.6 (5.1)	10.5 (5.1)
R_{pim}	0.048 (0.534)	0.049 (0.121)	0.055 (0.187)
Wilson B-value (Å^2)	31.652	27.61	21.54
Refinement statistics			
Resolution range (Å)	35.0-1.85	21.0-1.9	23.0-2.0
Reflections used (#)	43951	19026	34679
Free R reflections (%)	5.0	5.2	5.0
R/R_{free}	0.1687/0.1978	0.2208/0.2446	0.1452/0.1893
Rmsd bond length (Å)	0.012	0.008	0.008
Rmsd bond angle (°)	1.42	1.31	1.23
<B>	35.3	37.6	27.0
Ramachandran (%)			
No. of residues in			
Favored regions	98.2	96.8	98.6
Outlier regions	0	0	0
PDB entry	6MJS	6MJT	6MJR

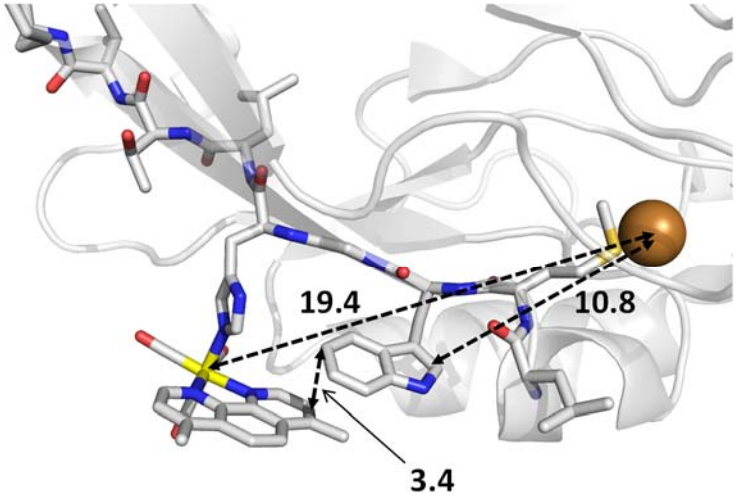

Figure S1. Structure of **Re124W122Cu^{II}**. From ref.[1] PDB: 2I7O. Distances in Å.
Note the near-parallel orientation of the dmp and indole planes that contain an angle of 20.8°.[1]

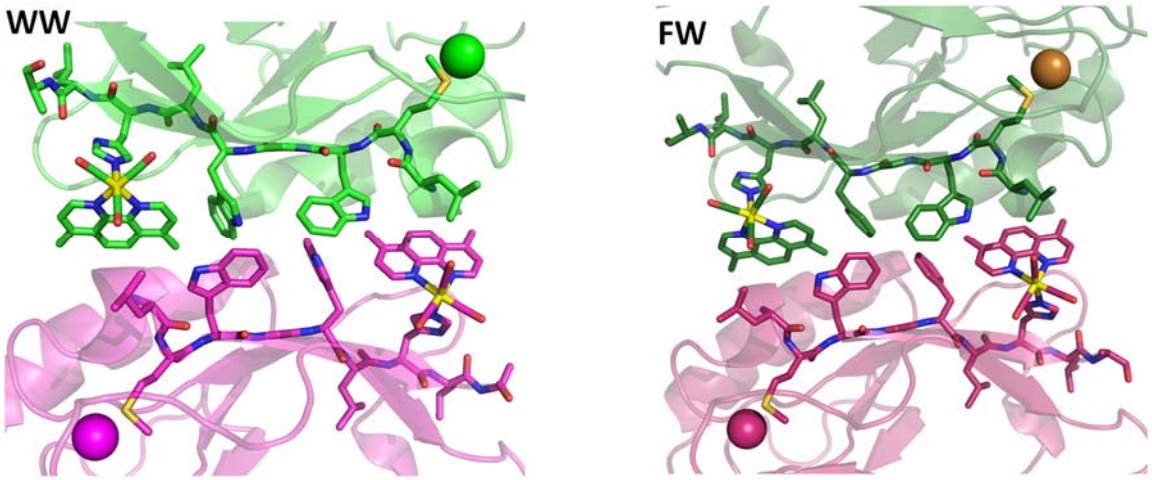

Figure S2. Packing of neighboring chains of **Re126WWCu^{II}** (left) and **Re126FWCu^{II}** (right) in the asymmetric unit. Note that the **Re126WWCu** interface (**WW**) provides intermolecular pathways for W122'→*Re, W122'↔W124, W122↔W124', and Re(H124)$(CO)_3$(dmp$^{\bullet-}$)→Cu(II)' ET, which may operate together with the intramolecular process. The **Re126FWCu** interface (**FW**) enables W122'→*Re intermolecular ET, making this mutant potentially photoactive at high concentrations in solution.

Section S2. Estimating single-step tunneling rates

Hopping acceleration is calculated as a ratio between the measured rate of Cu^{II} formation and the estimated rate of a hypothetical single-step process. Hence, the actual value depends on the way the latter is estimated.

We have used an experimental rate constant value for a single-step $Cu^{I} \rightarrow {}^{*}Re(His83)(CO)_3(phen)^{+}$ ET in Re-labeled WT azurin, 1.3×10^{6} s^{-1} (phen = 1,10-phenanthroline).[2] Assuming that the reaction occurs from a ^{3}MLCT excited state formally described as $^{*}Re^{II}(His126)(CO)_3(phen^{\bullet-})^{+}$, the ET distance was taken to be the crystallographically determined Cu-Re distance, 16.8 Å.[2] The hypothetical single-step rates in **Re124WCu^{I}** and **Re126WWCu^{I}** were calculated as $k_{ss} = (1.3\times10^{6})\exp(-\beta\Delta r)$, where β = 1.1 $Å^{-1}$ and Δr is the difference between the Cu-Re distances in the investigated hopping mutant and in Re(H83)(WT-azurin), as shown in Table S2a.

Table S2a. Estimating the single-step tunneling rates and acceleration factors in **Re124WCu^{I}** and **Re126WWCu^{I}** evaluated by comparison with Re(H83)-azurin.

	r(Re-Cu), Å	Δr, Å	k_{ss}	k_{Cu}	Acceleration
Re126WWCu^{I}	22.9	22.9-16.8=6.1	$(631\ \mu s)^{-1}$	$(70\ ns)^{-1}$	9 000
Re124WCu^{I}	19.4	19.4-16.8=2.6	$(13.4\ \mu s)^{-1}$	$(40\ ns)^{-1}$	336

An alternative way to estimate ET acceleration in **Re126WWCu^{I}** relative to **Re124WCu^{I}** relies on the ratio between measured single-step rate constants in flash-quench generated **Ru^{III}(H126)AzurinCu^{I}** (1.3×10^{2} s^{-1}) and **Ru^{III}(H124)AzurinCu^{I}** (2.2×10^{4} s^{-1}), as shown in Table S2b. Adjusting these values for different Ru-Cu and Re-Cu distances provides estimates of single-step rate constants for **Re126WWCu^{I} and Re124WCu^{I}** and indicates that single-step ET in **Re126WWCu^{I}** should be 21-times slower than in **Re124WCu^{I}**. Experimentally, it is only ~1.5-times slower, demonstrating the larger ET acceleration in **Re126WWCu^{I}**. It follows that ET acceleration in **Re126WWCu^{I}** is 15-times larger than in **Re124WCu^{I}**. Given the approximations involved in these estimates, this result corresponds well with the factor of 32 obtained from Table S2a.

Table S2b. Estimating the single-step tunneling rates and acceleration factors in **Re124WCu^{I}** and **Re126WWCu^{I}**. evaluated by comparison with Ru(H124)- and Ru(H126)-azurins. Distances in Å. k_s values from ref.[3-4]

	r(Re-Cu)	r(Ru-Cu)	Δr	k_{ss}, s^{-1} (Ru)	k_{ss}, s^{-1} (Re)	k_{Cu}	Acceleration
Re126WWCu^{I}	22.9	26.0	3.1	1.3×10^{2}	3.93×10^{3}	$(70\ ns)^{-1}$	3.6×10^{3}
Re124WCu^{I}	19.4	20.6	1.2	2.2×10^{4}	8.24×10^{4}	$(40\ ns)^{-1}$	3.0×10^{2}

The rate constant for $ReH126(CO)_3(dmp^{\bullet-})\rightarrow Cu^{II}$ back ET was estimated from the experimental value $(3.1\ \mu s)^{-1}$ of the analogous reaction in **Re124W122Cu^{I}**. Using Cu-Re and Cu-dmp distances (Table 1) produces values of 146 and 440 μs, respectively.

Section S3. Kinetics fitting and modeling

Kinetics fitting.

Luminescence decay and transient absorption kinetics were fit to multiexponential functions using the lsqnonlin function in Matlab (The Mathworks, Inc.). Luminescence decays from 5- and 50-ns streak camera timebases, and logarithmically spaced data from the 10-μs digitizer timebase of the nanosecond instrument, were spliced together to make single luminescence decay profiles spanning the time range from 50 ps to 10 μs. These data were fit to multiexponential functions by iterative reconvolution with an instrument response function. The data, fits, and residuals for **Re126WWCu^{I}**, **Re126WWCu^{II}**, **Re126WFCu^{I}**, **Re126FWCu^{I}**, and **Re126WWZn^{2+}** appear in Figures S3-S7. The fitting parameters are summarized in Table S3. Nanosecond transient absorption data recorded at 632.8 and 500 nm with **Re126WWCu^{I}** were fit simultaneously to a 4-exponential function. Nanosecond transient absorption data recorded at 500 nm with **Re126FWCu^{I}**, **Re126WFCu^{I}**, and **Re126WWZn^{2+}** were fit to exponential functions. The data, fits, and residuals appear in Figures S8-S11. The fitting parameters are summarized in Table S4.

Table S3. Amplitudes (A_i) and time constants (τ_i) from multiexponential fits to Re126-azurin luminescence decay kinetics.

	A_1 /%	τ_1 /ps	A_2 /%	τ_2 /ns	A_3 /%	τ_3 /ns	A_4 /%	τ_4 /μs
Re126WWCu^{I}	61±3	270±20	15±2	3.7±1	23±1	81±6		
Re126WWCu^{II}	71±1	290±10	9±1	4±2	20±2	79±7		
Re126WFCu^{I}	73±2	200±10	14±1	2.9±0.6	13±1	71±8		
Re126FWCu^{I}	36±6	340±100	14±6	3±2	5±4	120±100	45±5	1.16±0.15
Re126WWZn^{2+}	45±2	430±40	18±2	9.5±3	36±2	100±10		

Table S4. Amplitudes (A_i) and time constants (τ_i) from multiexponential fits to Re126-azurin nanosecond transient absorption kinetics.

Re126WWCu^{I}	A_1	τ_1	A_2	τ_2	A_3	τ_3	A_4	τ_4
TA 632.8 nm	−0.011	68±3 ns	0.005	1.2±0.1 μs	0.020	123±2 μs	0.002	4.6±0.5 ms
TA 500 nm	0.004		0.003		0.008		0.0008	
Re126FWCu^{I}								
TA 500 nm	0.005	1.1±0.15 μs	0.001	20±10 μs	0.0008			
Re126WFCu^{I}								
TA 500 nm	0.004	0.9±0.1 μs	0.0007					
Re126WWZn^{2+}								
TA500 nm	0.008	125±30 ns	0.001	4±3 μs	0.0005			

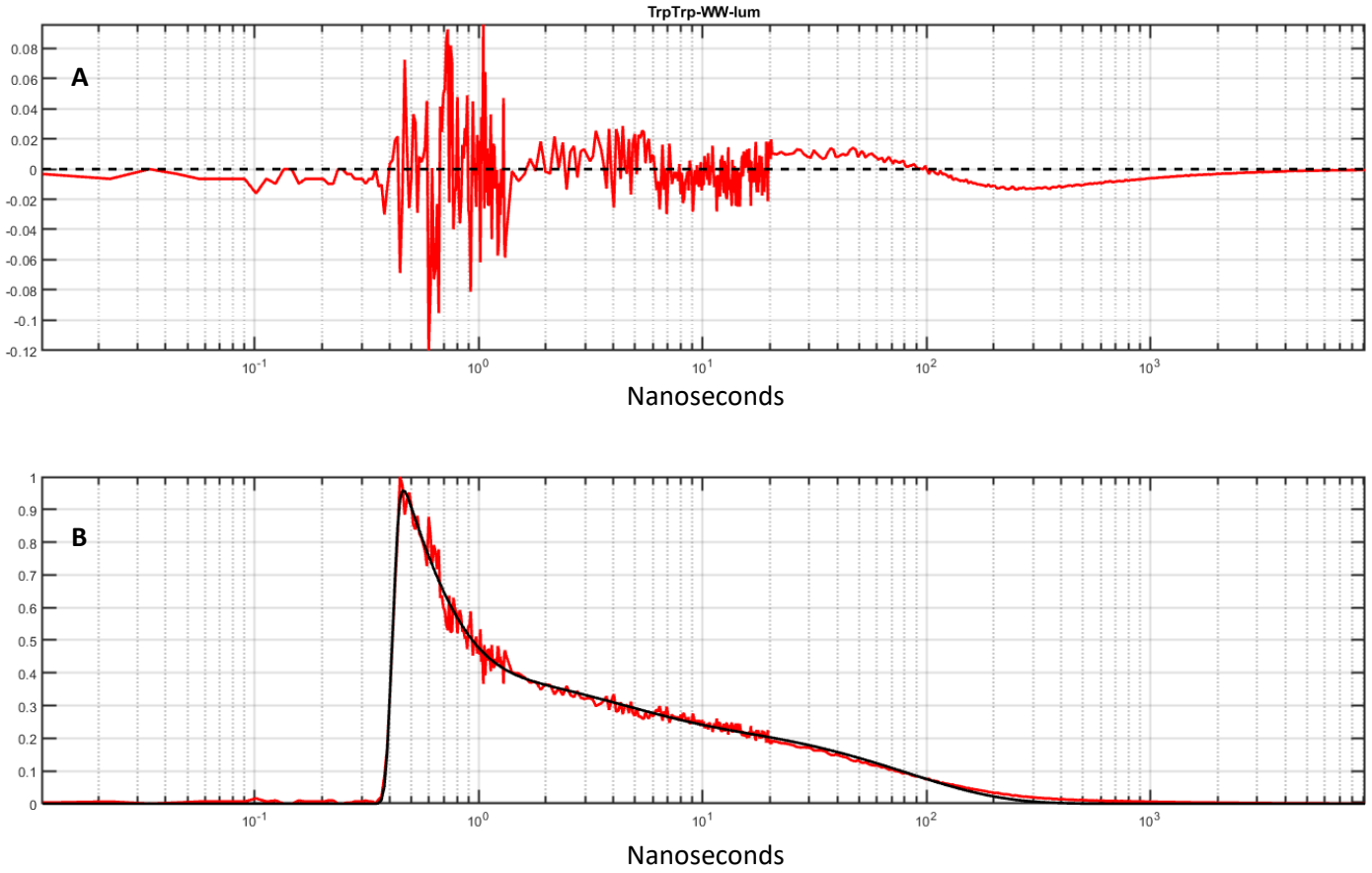

Figure S3. Luminescence decay kinetics of **Re126WWCu**^{I} (B, red), iterative reconvolution fit to 3-exponential decay function (B, black), and residuals (calculated−observed) (A).

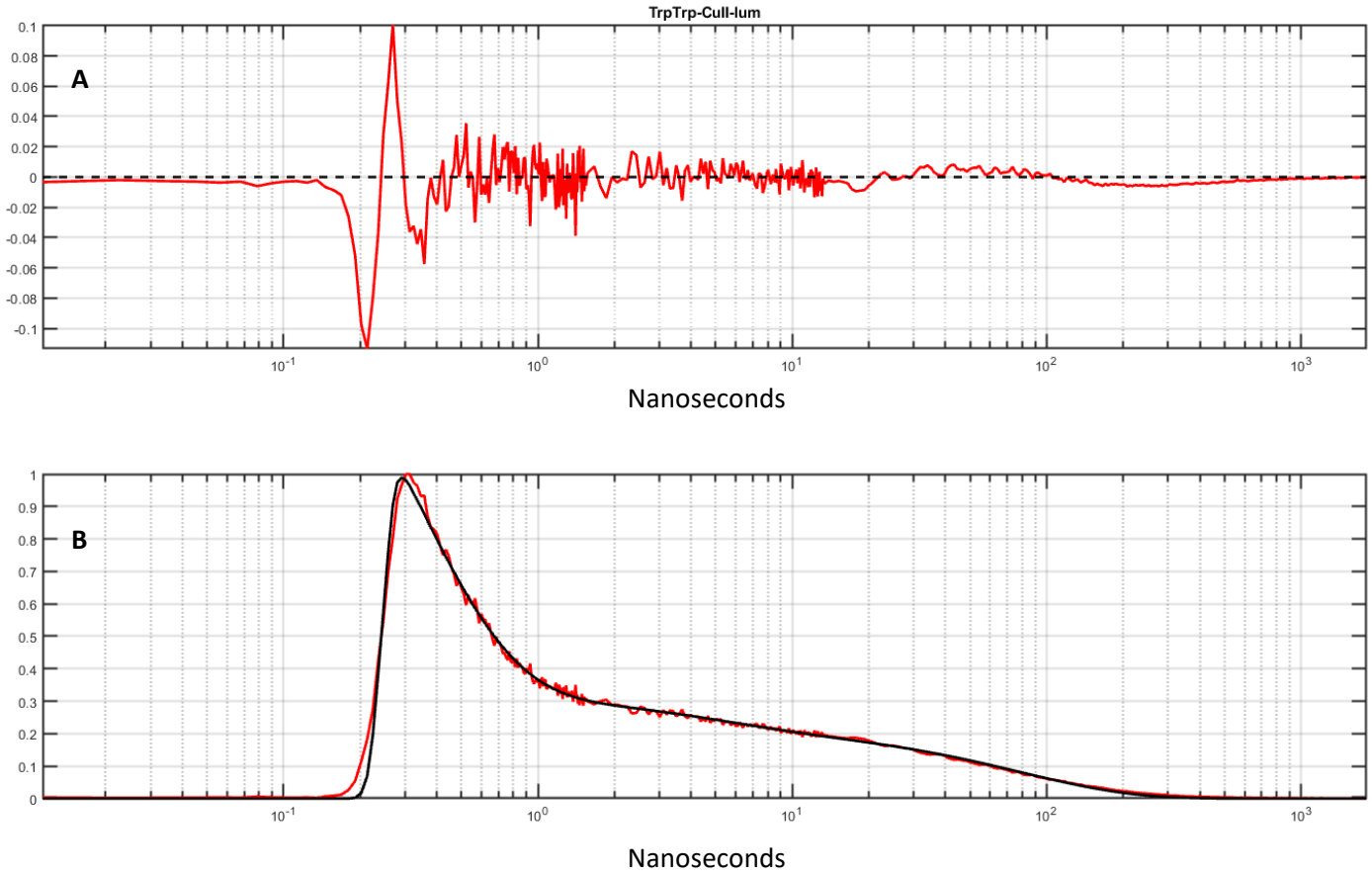

Figure S4. Luminescence decay kinetics of **Re126WWCu^{II}** (B, red), iterative reconvolution fit to 3-exponential decay function (B, black), and residuals (calculated−observed) (A).

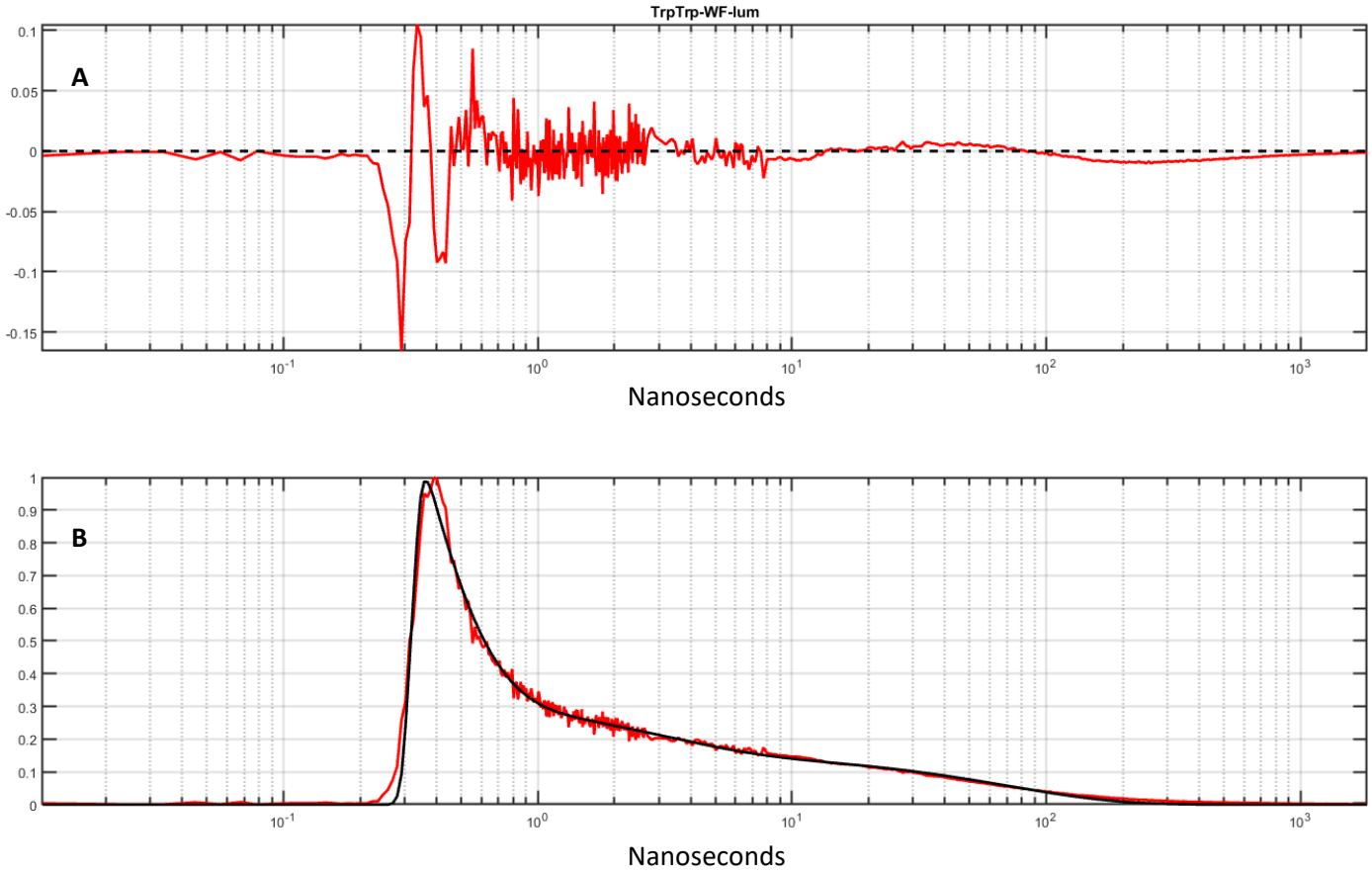

Figure S5. Luminescence decay kinetics of **Re126WFCu**^{I} (B, red), iterative reconvolution fit to 3-exponential decay function (B, black), and residuals (calculated−observed) (A).

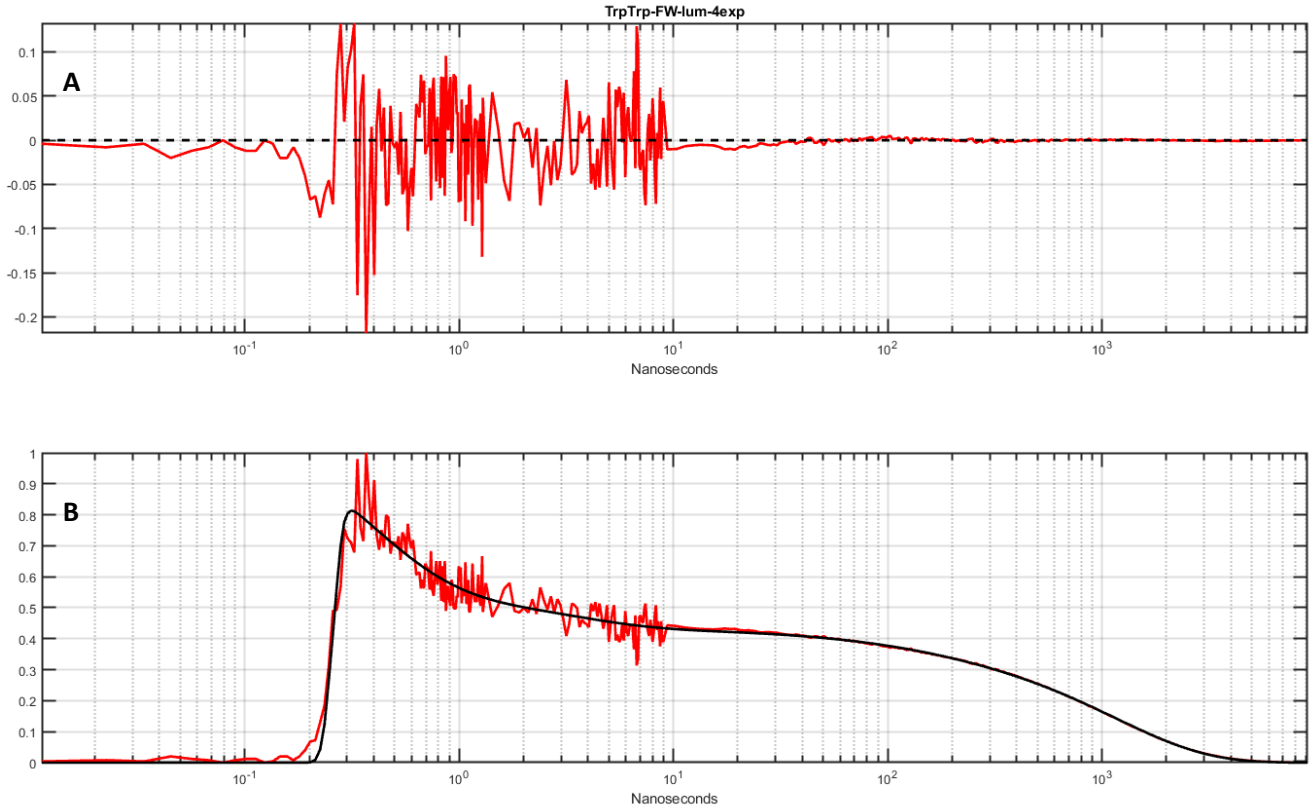

Figure S6. Luminescence decay kinetics of **Re126FWCu^{I}** (B, red), iterative reconvolution fit to 4-exponential decay function (B, black), and residuals (calculated−observed) (A).

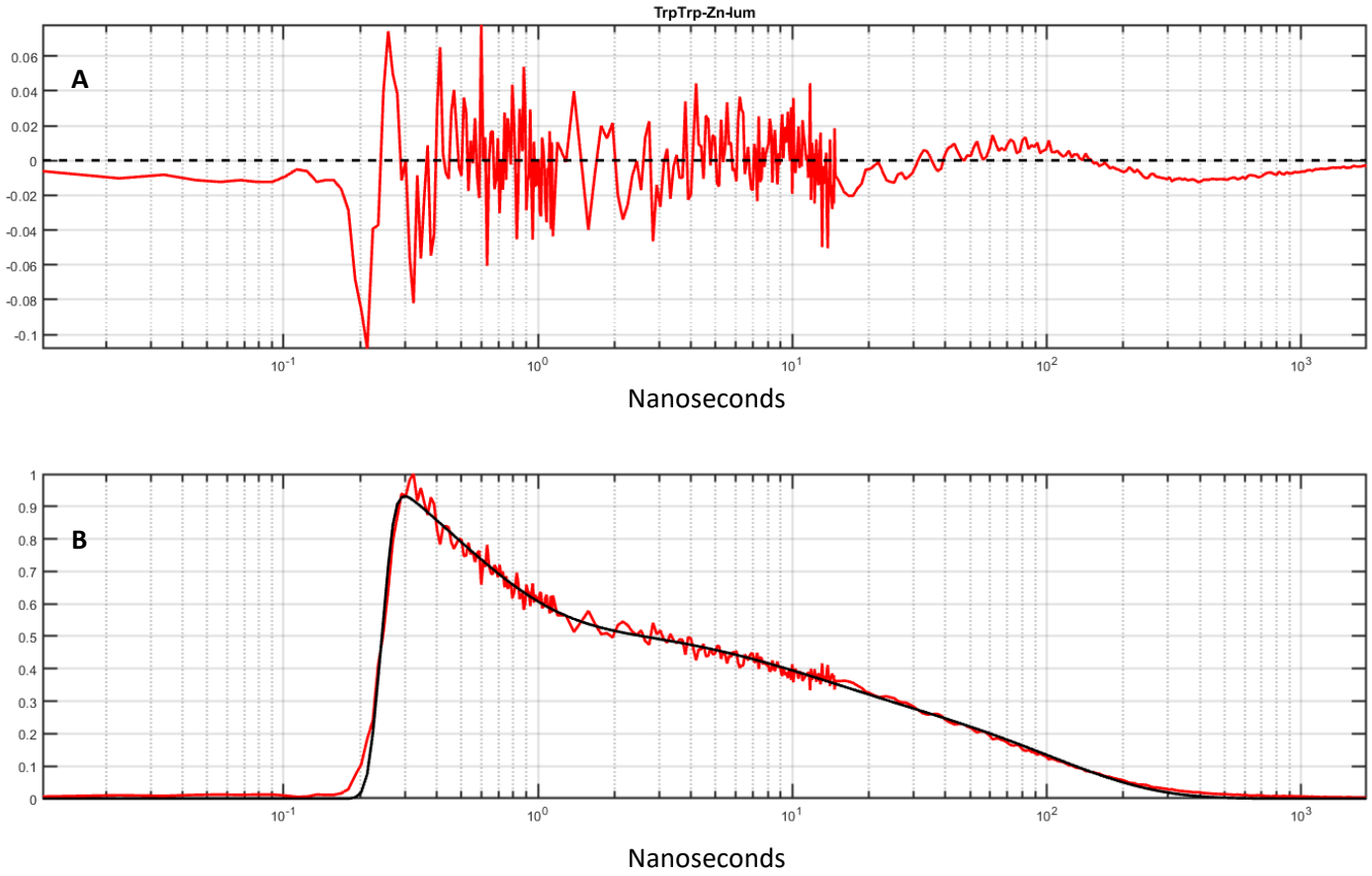

Figure S7. Luminescence decay kinetics of **Re126WWZn^{2+}** (B, red), iterative reconvolution fit to 3-exponential decay function (B, black), and residuals (calculated−observed) (A).

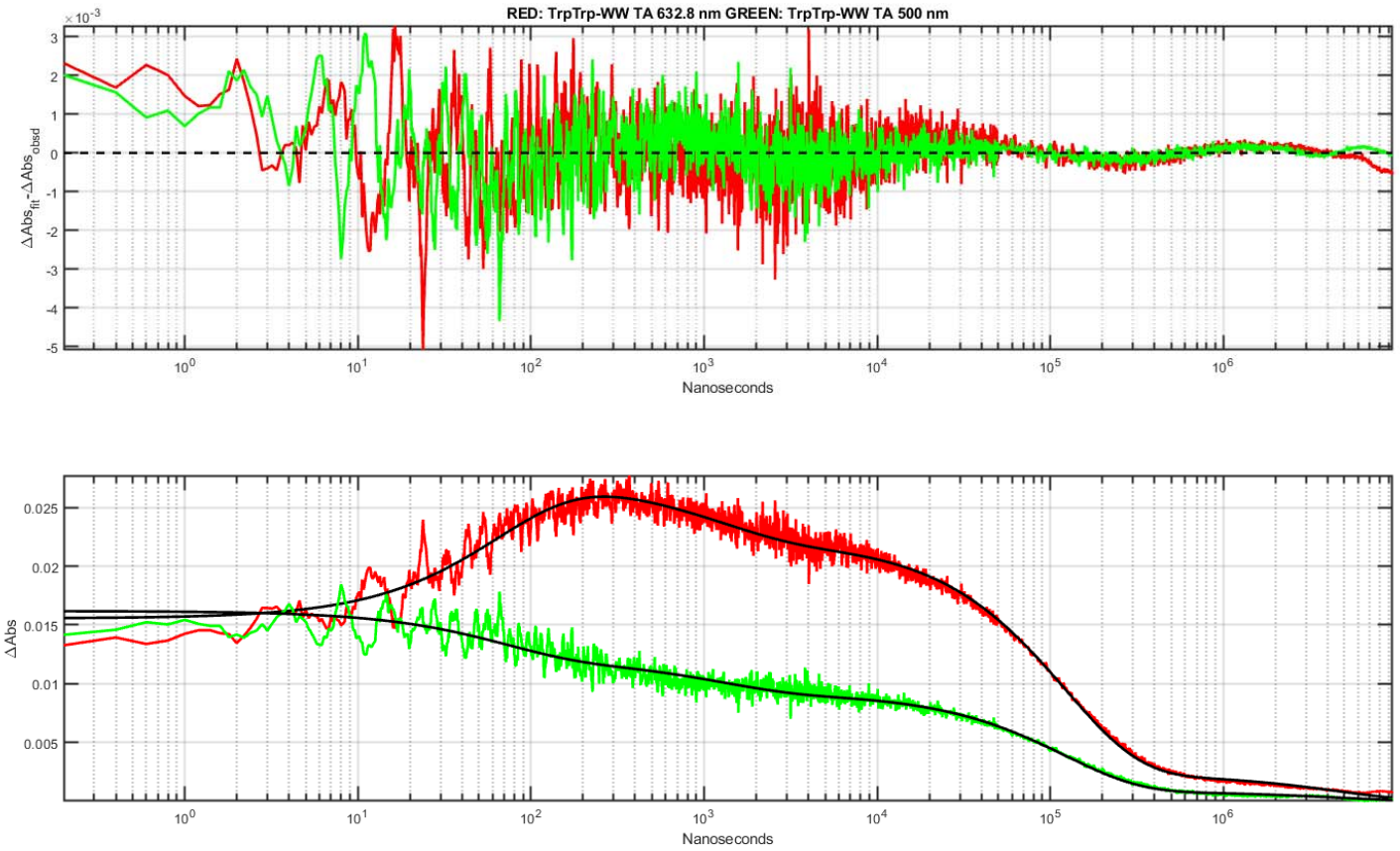

Figure S8. Nanosecond transient absorption kinetics of **Re126WWCu**^{I} recorded at 632.8 nm (B, red) and 500 nm (B, green), simultaneous fit to 4-exponential decay function (B, black), and residuals (calculated−observed) (A).

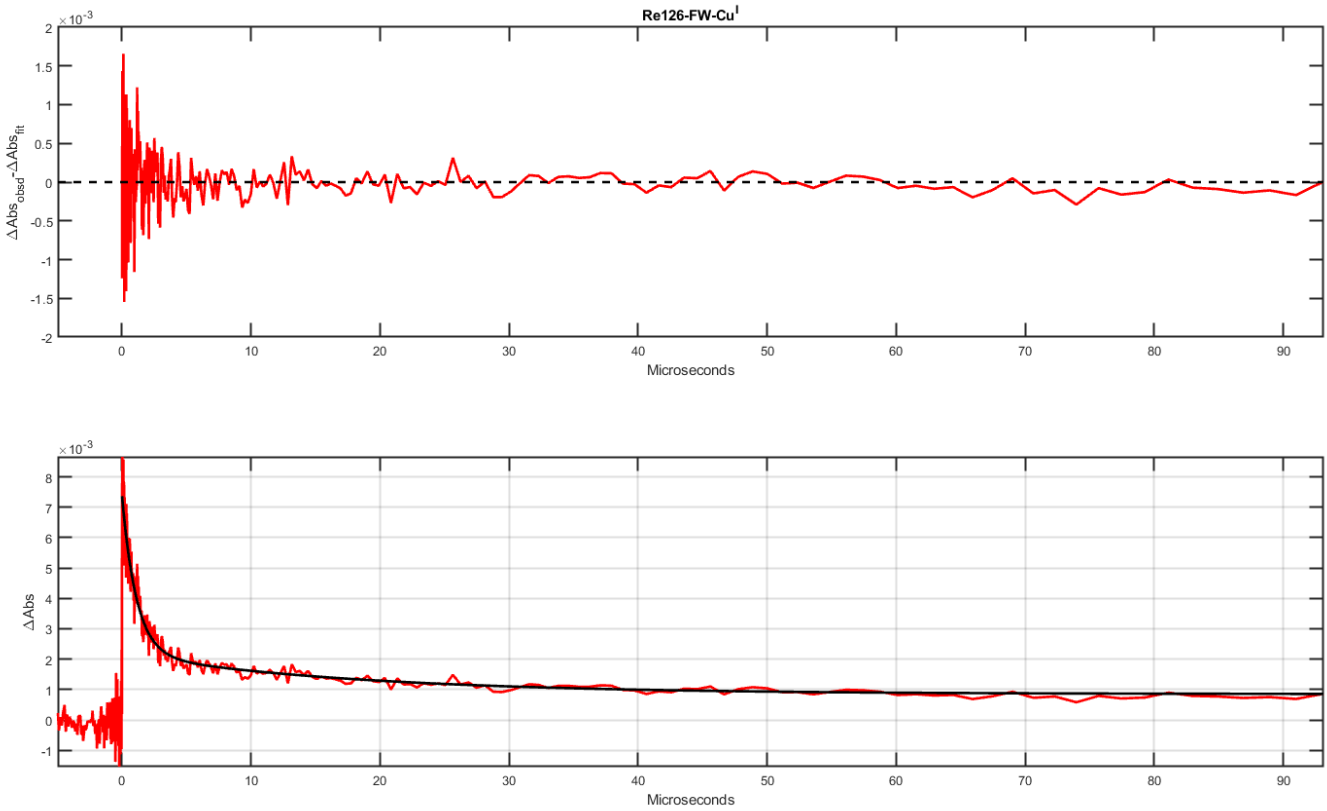

Figure S9. Nanosecond transient absorption kinetics of **Re126FWCu**^{I} recorded at 500 nm (B, red), fit to 2-exponential decay function (B, black), and residuals (observed−calculated) (A).

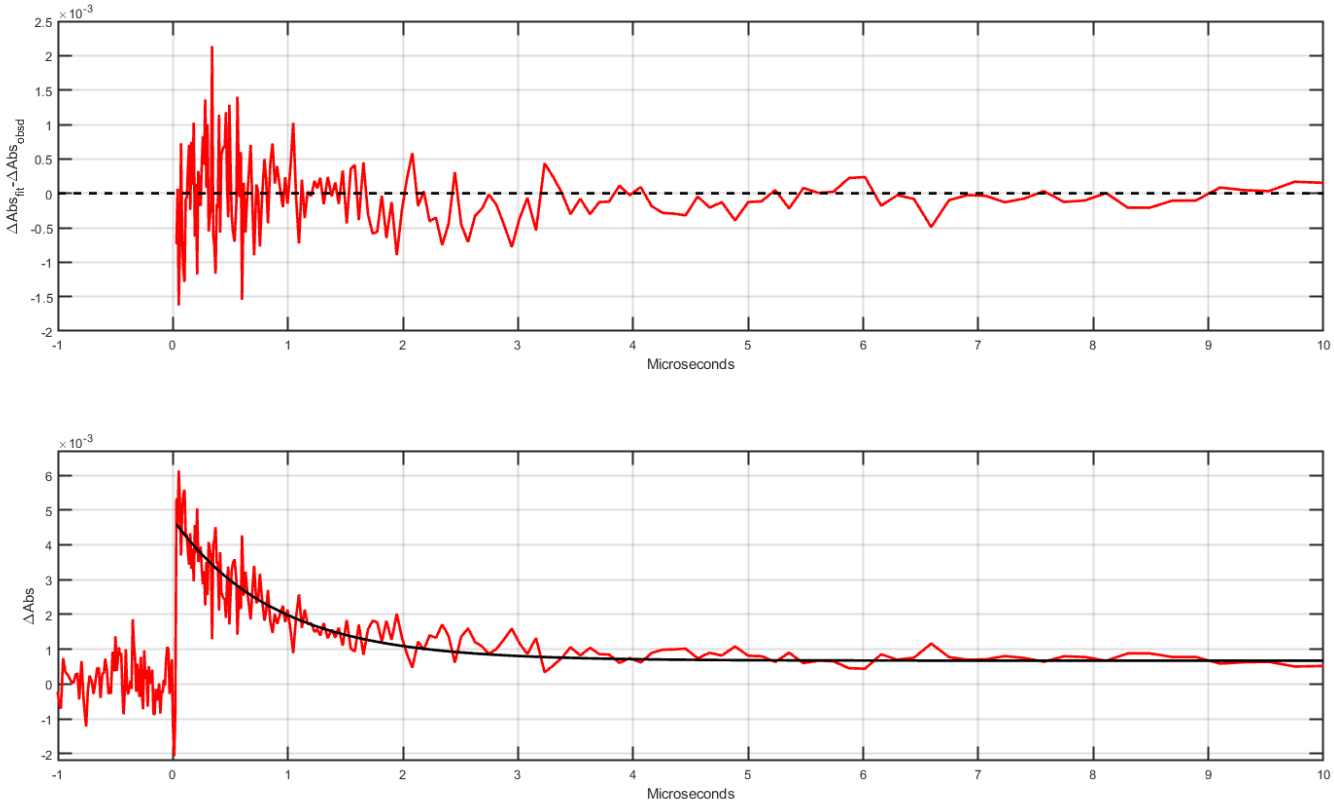

Figure S10. Nanosecond transient absorption kinetics of **Re126WFCu^{I}** recorded at 500 nm (B, red), fit to single-exponential decay function (B, black), and residuals (calculated−observed) (A).

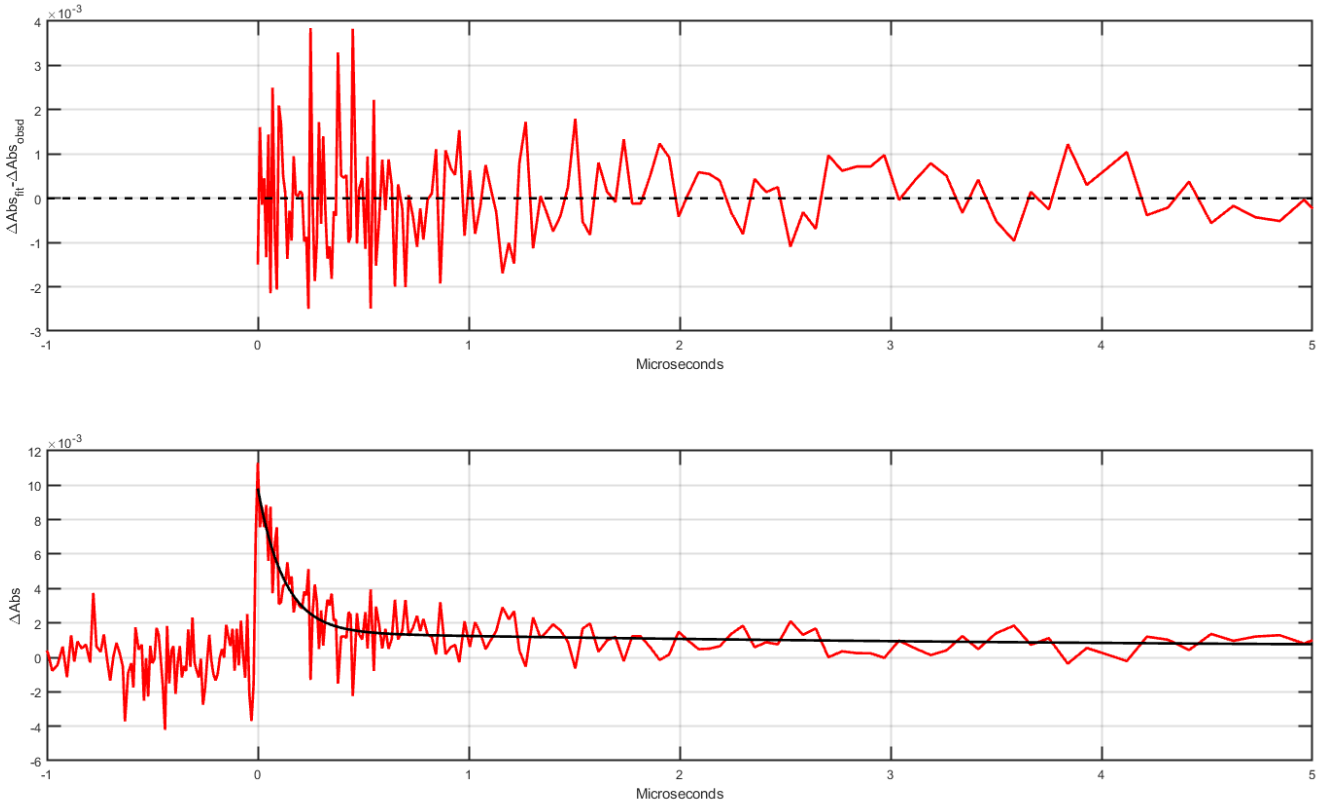

Figure S11. Nanosecond transient absorption kinetics of **Re126WWZn^{2+}** recorded at 500 nm (B, red), fit to 2-exponential decay function (B, black), and residuals (calculated−observed) (A).

Kinetics Modeling

A general mechanistic model for electron transport in Re126-azurins is outlined in Scheme S1. The limited number of experimental observations precludes unique determination of the 9 elementary rate constants indicated in the model.

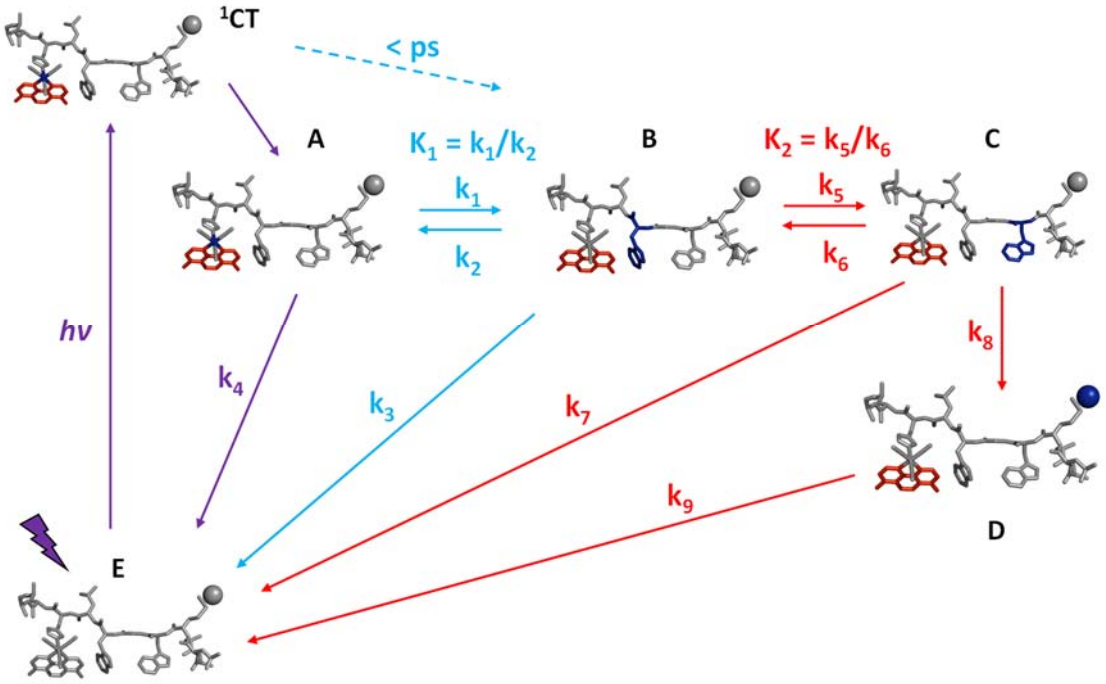

$$\frac{d[A]}{dt} = -(k_1 + k_4)[A] + k_2[B]$$
$$\frac{d[B]}{dt} = k_1[A] - (k_2 + k_3 + k_5)[B] + k_6[C]$$
$$\frac{d[C]}{dt} = k_5[B] - (k_6 + k_7 + k_8)[C]$$
$$\frac{d[D]}{dt} = k_8[C] - k_9[D]$$
$$\frac{d[E]}{dt} = k_4[A] + k_3[B] + k_7[C] + k_9[D]$$

Scheme S1. Kinetics scheme of intramolecular ET in **Re126WWCu^I** used to estimate elementary rate constants. The ET steps relevant for **Re126FWCu^I** and **Re126WFCu^I** are shown in purple and purple+blue, respectively.

The general solution to the five coupled first-order differential equations in Scheme S1 is a 4-exponential function. One of the empirical rate constants in the solution is equal to the elementary rate constant k_9. The remaining empirical rate constants are functions of $k_{1\text{-}8}$, given

by the roots of a third-order polynomial. Some of the elementary rate constants can be determined by comparisons to model compounds as outlined below.

1. The value of the rate constant k_4 was fixed equal to the **Re126FWCu^{I}** luminescence decay rate constant: k_4^{-1} = 1.15 μs.
2. Luminescence decay in **Re126WFCu^{I}** corresponds to Scheme S1 with $k_{5\text{-}9}$ = 0. This rate law can be solved analytically and, using the experimental luminescence amplitudes and rate constants, the following assignments can be made: k_1^{-1} = 234 ns; K_1 = 5.7; k_3^{-1} = 61 ns.

To model the kinetics in **Re126WWCu^{I}**, 3 elementary rate constants were fixed (k_3^{-1} = 60 ns, k_4^{-1} = 1.15 μs, k_9^{-1} = 120 μs). The remaining 6 rate constants were varied systematically and used to provide numerical solutions to the Scheme S1 differential equations with the initial condition $[A]_0$ = 1; $[B]_0$ = $[C]_0$ = $[D]_0$ = $[E]_0$ = 0. The set of rate parameters used in solving the differential equations was:

k_1^{-1} = 200 – 750 ps
K_1 = 1 – 5
k_5^{-1} = 1 – 25 ns
K_2 = 0.1 – 0.75
k_7^{-1} = 100 – 750 ns
k_8^{-1} = 40 – 100 ns.

The observations used to test the solutions were the rate constants extracted from the luminescence and transient absorption data, the relative amplitudes of the luminescence kinetics phases, and the yield of Cu^{II} formed in the hopping process. The relative Cu^{II} yield was estimated from the experiment shown in Figure 2B: Kinetics profiles of transient absorption of **Re124W122Cu^{I}** and **Re126WWCu^{I}** at 633 nm were measured on the same day at virtually identical experimental conditions and normalized for the absorbance at the 355 nm excitation wavelength. The relative yield was determined as the ratio of the amplitude of the respective decay kinetics components. Whereas the **Re124W122Cu^{I}** 633 nm TA decays with single-exponential ~3.4 μs kinetics (3.1 μs in ref.[1]), **Re126WWCu^{I}** shows biexponential 1.2 and 123 μs decay (Table 2) due to inter- and intramolecular reactions, respectively. Considering only the 123 μs decay, the Re124/Re126 relative yield was estimated as 1.7, without knowing the partial light absorption that triggers intramolecular reactivity. The total relative yield (calculated from both 1.2 and 123 μs amplitudes) is 2.4. The actual value corresponding to the intramolecular process lies in the 1.7-2.4 range.

Systematic variation of the six rate parameters required solution of 4.8×10^7 systems of differential equations. The following criteria were employed to screen for acceptable solutions:

Cu^{II} yield: 2.0 – 2.2
τ_1: 260 – 280 ps
τ_2: 3.5 – 4 ns
τ_3: 70 – 90 ns
τ_4: 120 μs

The time constants τ_i are reciprocals for the four empirical rate constants in the solution to the differential equations. The resulting elementary rate constants are listed in Table 3 of the main text.

Summary of mechanistic aspects:

(i) The CT ⇌ CS1 equilibrium and the W124→*Re forward ET rate constants in **Re126WWCu^{I}** are close to those estimated[1] for **Re124W122Cu^{I}** (2.8, 500 ps), despite different dmp/indole orientations.
(ii) W124 and W122 are distinct hopping intermediates, as opposed to a single highly delocalized {W124,W122} unit. (For the latter possibility, the simulations predicted too high Cu^{II} relative yields, unless the recombination rate constant ($k_3 = k_7$) was unrealistically large.)
(iii) The CS1 ⇌ CS2 equilibrium is shifted to the left ($K_2 \cong 0.55 – 0.75$), i.e., the hole-localization on W124 proximal to Re is thermodynamically preferred.
(iv) The W122→$W124^{\bullet+}$ (CS1 → CS2, k_5) and $Re^{I}(H126)(CO)_3(dmp^{\bullet-})$→$W124^{\bullet+}$ (CS2 → GS) steps are much faster and slower, respectively, than Cu^{I}→$W124^{\bullet+}$ ET (CS2→RP, $k_8^{-1} \cong$ 60-90 ns). Hence, they do not affect the luminescence decay and Cu^{II} formation kinetics and their rate constants cannot be determined from the present experiments.
(v) Comparison with parameters estimated for **Re126WWCu^{II}** (k_1^{-1} = 375-425 ps^{-1}, K_1 = 2.25-3.25, k_3^{-1} = 60 ns, k_4^{-1} = 1.15 μs, k_5^{-1} = 9-21 ns, K_2 = 0.25-0.75, k_7^{-1} = 30 ns) indicate that the kinetics and thermodynamics of the ^{3}CT ⇌ CS1 ⇌ CS2 redox processes are nearly independent of the Cu oxidation state (and, presumably, also of replacing Cu^{II} by Zn^{II}).
(vi) Parameters estimated for **Re126WFCu^{I}** (k_1^{-1} = 234 ps, K_1 = 5.7, k_3^{-1} = 61 ns) show that initial ^{3}CT ⇌ CS1 equilibrium (i.e., W124→*Re ET) is only little affected by the 122 residue.

Section S4. QM/MM dynamics simulations

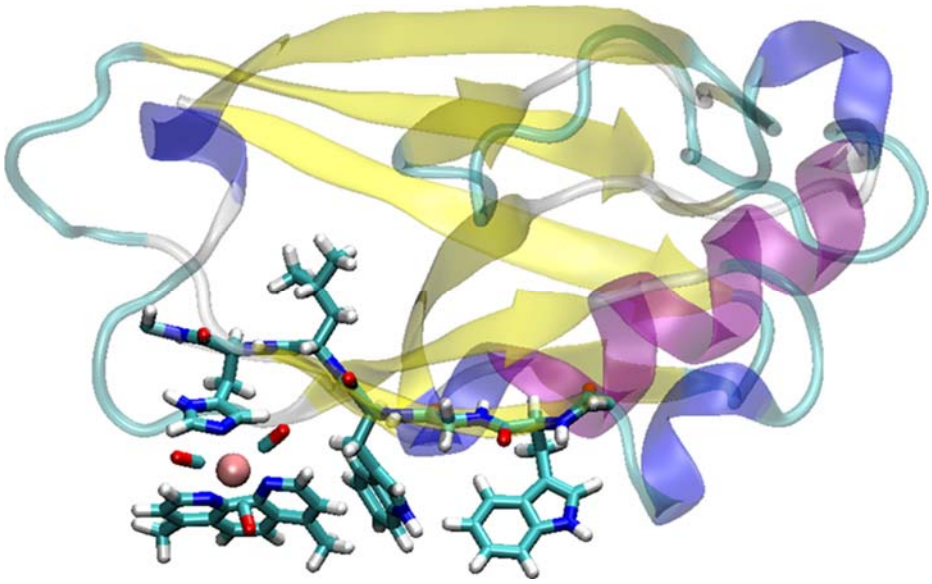

Figure S12. Re126WWCu^{I} used QM/MM MD simulations of complexes. The QM (DFT/PBE0-D3) part is shown in a licorice representation, the rest of the protein is treated by MM. Water molecules included in the MM part are omitted for simplicity.

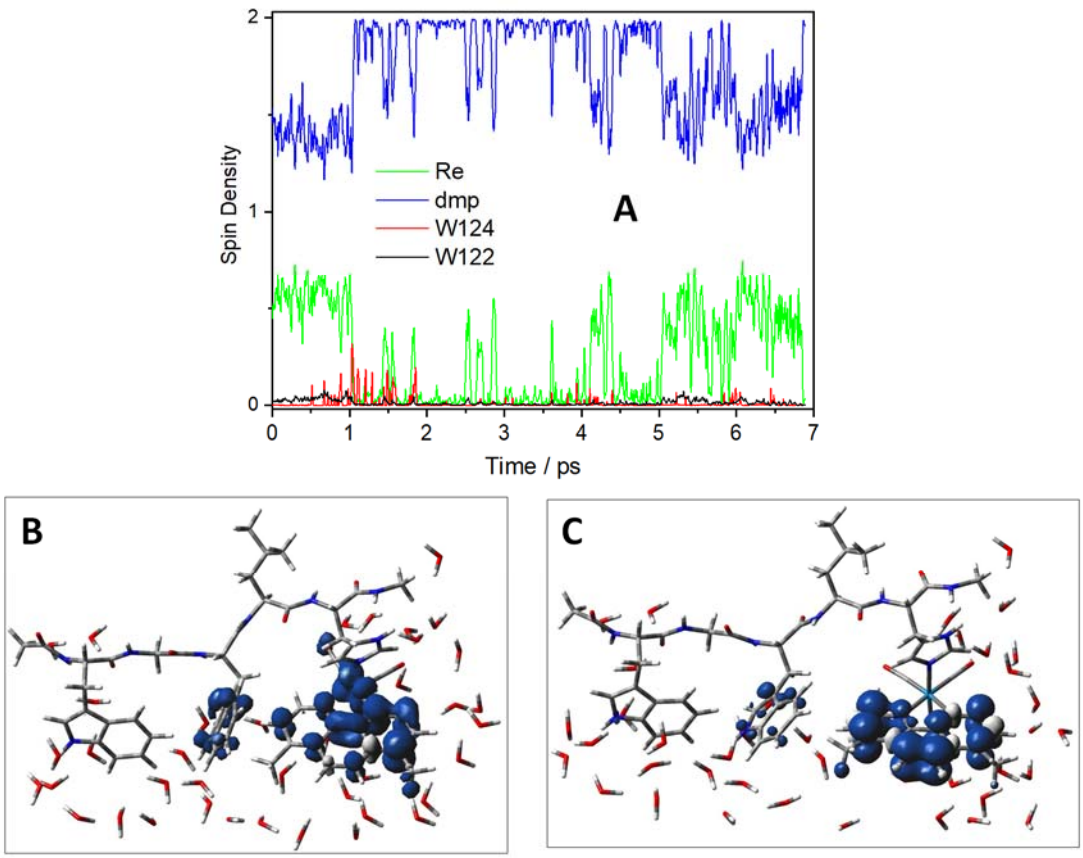

Figure S13. Character and dynamics of the ^{3}CT excited state of **Re126WWCu^I**. **A**: Time-dependent spin density distribution of the lowest triplet state (^{3}CT) from UKS QM/MM/MD simulation of the complete system, starting from the optimized ^{3}CT geometry. **B**: UKS-calculated spin density distribution at 0.3 ps where the lowest triplet is predominantly MLCT. **C**: UKS-calculated spin density distribution at 1.2 ps, where the lowest triplet is predominantly IL. Spin density distributions in **B** and **C** were calculated on the QM part of the system solvated with nearby 40 water molecules and embedded in bulk water described as a polarizable continuum.

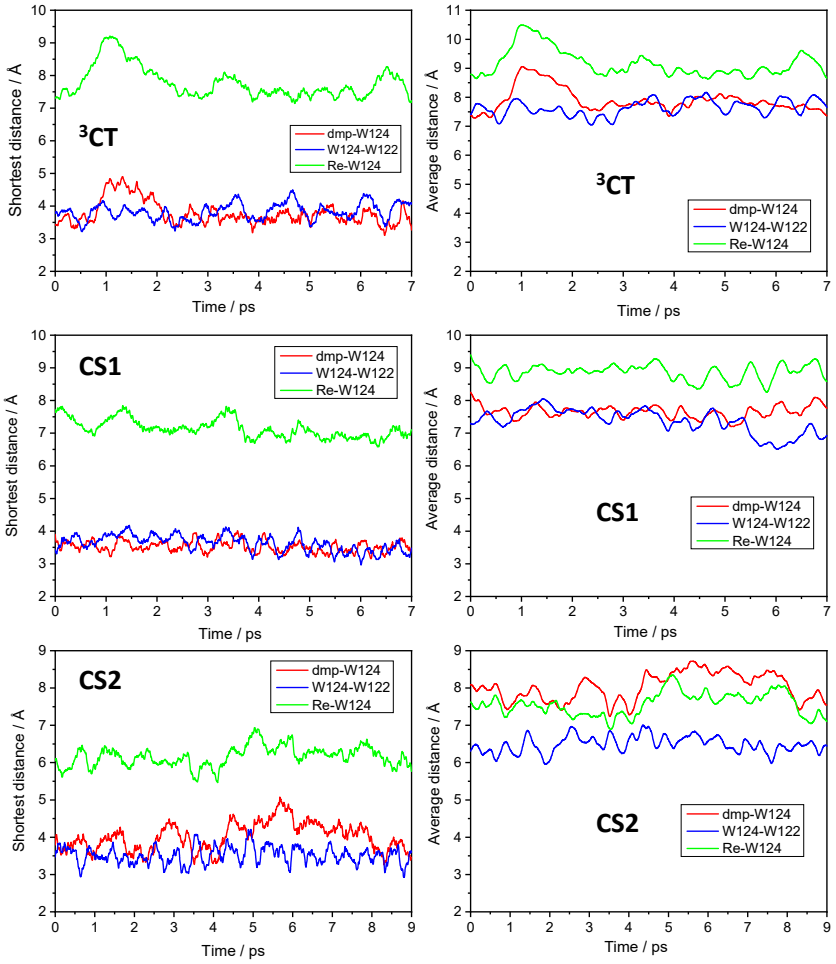

Figure S14. Distances between redox cofactors in solvated **Re126WWCu^I** along UKS/MD trajectories of ^{3}CT, CS1, and CS2 states.

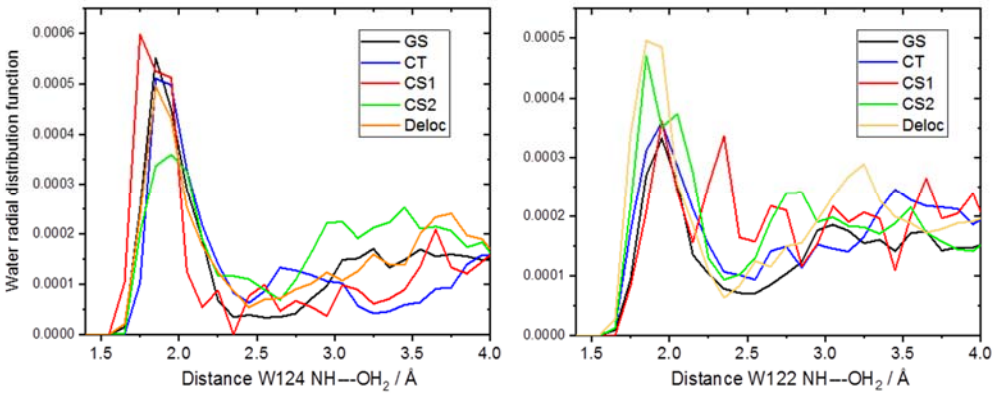

Figure S15. Radial water distribution function around the W124 (left) and W122 (right) indole-NH hydrogen atoms in various electronic states of **Re126WWCu**^{I}. Solvation tightening is manifested by shifting the strong peak around 2 Å to shorter distances and increasing its height. NH-O distance distribution for individual water molecules is shown in Figure 4. It follows that oxidation of either tryptophan is accompanied by H-bonding and tighter solvation. In particular, W124 solvation is about the same in the ground- and ^{3}CT states but tightens upon oxidation to W124$^{\bullet+}$ in the CS1 state where the NH---OH_2 distance shortens by about 0.1 Å. Restoring the W124 neutral charge on going to CS2 results in a shift of solvating water toward W122$^{\bullet+}$. This shift is accompanied by the emergence of a second solvation layer between 3.0-3.5 Å around W124. Opposite behavior was found for W122, whose solvation is similar in the ground-, ^{3}CT and CS1 states but becomes tighter in CS2, where the NH group is strongly bound to a single water molecule.

Section S5. Materials and methods

Protein expression and labeling. Site-directed mutagenesis K122W/T124W/T126H, K122F/T124W/T126H, and K122W/T124F/T126H of plasmid *Pseudomonas aeruginosa* Az All-Phe H83Q/Y72F/Y108F/W48F (All-Phe refers to replacement of all native W or Y with F) was carried out using a QuickChange kit (Stratagene). Primers were purchased from Operon. Mutant azurins were expressed in BL21(DE3) *E. coli.* cells, purified, and labeled with the Re complex according to a literature procedure:[5] $[Re(H_2O)(CO)_3(dmp)](OTf)$ and protein were incubated in HEPES buffer at 37°C for 4-7 days in a 1.5:1.0 ratio before being exchanged into NaP_i buffer. Labeled protein was isolated from unlabeled protein using an IMAC copper-chelating column, followed by purification on a Mono S cation exchange column. Final products were characterized by electrospray ionization mass spectrometry and UV/vis absorption spectroscopy.

X-ray crystallography. Crystals were obtained by sitting-drop vapor diffusion. For **Re126WWCu^{II}**, 8 mg/mL in solution of 40 mM imidazole buffer at pH 7.2 with 2 mM NaCl were mixed with well solution (100 mM imidiazole, 100 mM $LiNO_3$, 6.25 mM $CuCl_2$, 28% PEG 4000) in a 1:1 ratio (vol/vol). For **Re126WFCu^{II}** and **Re126FWCu^{II}**, 14.5 mg/mL in solution of 20 mM NaP_i buffer at pH 7.6 with 1 M NaCl were mixed with well solutions (0.1 M NaOAc, 120 mM/150 mM Li_2SO_4, and 48.6% PEG 400/27.7% PEG 8000 at pH 4.5) in 1:1 ratios (vol/vol) respectively. Crystals were harvested after 4d-2wk and cryogenically stored. X-ray diffraction data were collected on the Stanford Synchrotron Radiation Laboratory (SSRL) Beamline 12-2 for **Re126WWCu^{II}** and on an in-house instrument (Rigaku Micromax-007 HF & R-axis IV++) for the other two mutants. Diffraction data were processed with XDS/iMosflm/Scala,[6-7] while the structures were solved using Phaser, Coot, and Phenix.[8-10] Statistics for data collection and refinement are show in **Table S1**. Atomic coordinates and structure factors were deposited in the Protein Data Bank under entries: **6MJR, 6MJS, 6MJT**

Time-resolved luminescence and TA spectroscopy Laser experiments were conducted at the Beckman Institute Laser Resource Center at Caltech. Samples (15-40 μM) were reduced using either sodium dithionite or ascorbic acid and desalted using PD-10 columns into 25 mM NaP_i buffer at pH 7.2. After deoxygenation by pump-backfill cycles with argon, samples were excited by the third-harmonic of either a Q-switched Nd:YAG laser (Spectra Physics, Quanta-Ray PRO-Series, 8 ns pulse width) or a regeneratively amplified passively mode-locked Nd:YAG laser (Spectra Physics Vanguard 2000 and Continuum Regenerative Amplifier RGA60, 10 ps pulse width) for ns/μs and ps/ns-timescale measurements, respectively. For TA measurements, probe light was provided by either a current-pulsed Xe arc lamp (500/630 nm) or a HeNe laser (632.8 nm). For TA and luminescence experiments on the ns/μs-timescale, light was detected by a photomultiplier tube. For faster timescale measurements, a streak camera (Hamamatsu C5680) was used in photon-counting mode. Time-resolved IR experiments were performed at the Lasers for Science Facility, STFC Rutherford Appleton Laboratory (UK) using the ULTRA instrument.[11] TRIR spectra in the ps and ns range were measured using 400 (~50 fs fwhm) and 355 nm (~0.7 ps fwhm) excitation pulses, respectively, and probed with difference-frequency generated ~400 cm^{-1} broad IR probe pulses, recorded on two 128-pixel detectors with ~2 cm^{-1} spectral resolution. Samples were held in CaF_2 cells (Hellma) with a 50 μm path length.

Computational details. Molecular dynamics (MD) simulations of lowest triplet states of **Re126WWCu**^{I} were performed at quantum mechanical/molecular mechanical (QM/MM) level in Terachem 1.9[12-13] – Amber 14[14] framework. Simultaneous calculations of several low-lying triplet states utilized time-dependent DFT (TDDFT) with a closed shell reference state. Individual triplet states were calculated by an unrestricted Kohn-Sham (KS) procedure (UKS).[15] Snapshot calculations at individual points of MD trajectories were performed using Terachem 1.9 or Gaussian 16[16] (G16) program packages. Calculations of the QM part utilized LAN2DZ quasirelativistic effective core pseudopotentials and a corresponding optimized set of basis functions for Re[17] and 6-31g(d) polarized double-ζ basis sets[18] for remaining atoms. DFT employed the PBE0 hybrid functional,[19-20] together with an empirical dispersion correction D3.[21] Test calculations with long-range functionals CAM-B3LYP and wB97XD led to unrealistically large CT-CS energy separations.

The initial modeled complex structure containing a single protein chain with the Re-complex was based on the crystal structure (PDB ID 6MJS). The QM region contained residues 122-126 (W-G-W-L-H) and the Re-complex; the rest of the system is the MM region. The QM region was terminated by CH_3 groups thate were linked with the MM part through H atoms. This system was solvated by 3342 SPC/E[22] water molecules, resulting in minimum 6 Å water shell; 2 Na^+ cations[23] were added to compensate the charge of the protein chain. We noted that QM/MM does not support periodic-boundary-conditions (PBC) and therefore a harmonic potential for all water molecules was employed to provide a spherical water "cap" around the protein. The whole solvated system was simulated as a large cluster in a gas phase.[24] Electrostatics were accounted for by a very large Coulomb cut-off. The solvent continuum within G16 was described by a polarizable continuum model (PCM).[25]

In the preparatory steps and equilibration of the MM part of the system, strict position restraints were employed on all atoms in the QM region, and the system was treated with PBC; particle mesh Ewald accounted for long range electrostatics.[24,26] Minimization of the MM part was performed in two steps. First, all protein atoms were restrained and only solvent was minimized, next, only protein heavy atoms were restrained and solvent molecules and hydrogen atoms were minimized. With the position restraints on heavy atoms, the system was gradually heated up to 300 K during 200 ps in the NVT simulation (at a density 0.75 kg/dm^3); and finally the water was equilibrated. The density reached ~1.04 kg/dm^3 during 500 ps of the NpT simulation at ambient conditions, employing a 2 fs time step. The SHAKE algorithm[27] was employed to all bonds that involve hydrogen atoms. The final system, with equilibrated solvent and relaxed protein MM part, was again minimized, with weak restraints applied only on atoms of the QM region. During the all-MM equilibration period, CO and dmp groups were parameterized using the recommended AMBER approach.[28] The RESP charges were calculated in G16 and obtained by the antechamber tool in Amber. The Cu atom was modeled on an MM level. To account for the Cu-coordination in the active site, bond-length constraints to all ligands with optimal QM-distances according the literature were employed.[29]

QM/MM started by minimization, in order to optimize the geometry of the QM-region. QM/MM-dynamic simulations were performed with a 1 fs time step (SHAKE algorithm was used.) During 1 ps equilibration, the system was heated from 50 to 300 K. This step was performed

separately for KS-singlet and UKS-triplet states and the final geometry served as initial geometry and velocities for the production phase. Production runs were performed at 300 K employing a simulation time up to 10 ps for each of the KS and UKS simulations, while it was 1-4 ps for more computationally demanding TD-DFT simulations.

References

1. Shih, C.; Museth, A. K.; Abrahamsson, M.; Blanco-Rodriguez, A. M.; Di Bilio, A. J.; Sudhamsu, J.; Crane, B. R.; Ronayne, K. L.; Towrie, M.; Vlček, A., Jr.; Richards, J. H.; Winkler, J. R.; Gray, H. B., Tryptophan-Accelerated Electron Flow Through Proteins. *Science* **2008,** *320*, 1760-1762.
2. Crane, B. R.; Di Bilio, A. J.; Winkler, J. R.; Gray, H. B., Electron Transfer in Single Crystals of Pseudomonas aeruginosa Azurins. *J. Am. Chem. Soc.* **2001,** *123*, 11623-11631.
3. Langen, R.; Chang, I.-J.; Germanas, J. P.; Richards, J. H.; Winkler, J. R.; Gray, H. B., Electron Tunneling in Proteins: Coupling Through a β Strand. *Science* **1995,** *268*, 1733-1735.
4. Gray, H. B.; Winkler, J. R., Electron tunneling through proteins. *Q. Rev. Biophys.* **2003,** *36*, 341-372.
5. Di Bilio, A. J.; Crane, B. R.; Wehbi, W. A.; Kiser, C. N.; Abu-Omar, M. M.; Carlos, R. M.; Richards, J. H.; Winkler, J. R.; Gray, H. B., Properties of Photogenerated Tryptophan and Tyrosyl Radicals in Structurally Characterized Proteins Containing Rhenium(I) Tricarbonyl Diimines. *J. Am. Chem. Soc.* **2001,** *123*, 3181-3182.
6. Kabsch, W., XDS. *Acta Cryst.* **2010,** *D66*, 125-132.
7. Kabsch, W., Evaluation of single-crystal X-ray diffraction data from a position-sensitive detector. *J. Appl. Cryst.* **1988,** *21*, 916-924.
8. McCoy, A. J.; Grosse-Kunstleve, R. W.; Adams, P. D.; Winn, M. D.; Storoni, L. C.; Read, R. J., *Phaser* crystallographic software. *J. Appl. Cryst.* **2007,** *40*, 658-674.
9. Emsley, P.; Cowtan, K., Coot: model-building tools for molecular graphics. *Acta Cryst.* **2004,** *D60*, 2126-2132.
10. Adams, P. D.; Mustyakimov, M.; Afonine, P. V.; Langan, P., Generalized X-ray and neutron crystallographic analysis: more accurate and complete structures for biological macromolecules. *Acta Cryst.* **2009,** *D65*, 567-573.
11. Greetham, G.; Burgos, P.; Cao, Q.; Clark, I. P.; Codd, P.; Farrow, R.; George, M. W.; Kogimtzis, M.; Matousek, P.; Parker, A. W.; Pollard, M.; Robinson, D.; Xin, Z.-J.; Towrie, M., ULTRA - A Unique Instrument for Time-resolved Spectroscopy. *Applied Spectroscopy* **2010,** *64*, 1311-1319.
12. Ufimtsev, I. S.; Martínez, T. J., Quantum Chemistry on Graphical Processing Units. 3. Analytical Energy Gradients and First Principles Molecular Dynamics. *J. Chem. Theor. Comp.* **2009,** *5*, 2619-2628.
13. Titov, A. V.; Ufimtsev, I. S.; Luehr, N.; Martínez, T. J., Generating Efficient Quantum Chemistry Codes for Novel Architectures. *J. Chem. Theor. Comp.* **2013,** *9*, 213-221.
14. Case, D. A.; Babin, V.; Berryman, J. T.; Betz, R. M.; Cai, Q.; Cerutti, D. S.; T.E. Cheatham, I.; Darden, T. A.; Duke, R. E.; Gohlke, H.; Goetz, A. W.; Gusarov, S.; Homeyer, N.; Janowski, P.; Kaus, J.; Kolossváry, I.; Kovalenko, A.; Lee, T. S.; LeGrand, S.; Luchko, T.; Luo, R.; Madej, B.; Merz, K. M.; Paesani, F.; Roe, D. R.; Roitberg, A.; Sagui, C.; Salomon-Ferrer, R.; Seabra, G.; Simmerling, C. L.; Smith, W.; Swails, J.; Walker, R. C.; Wang, J.; Wolf, R. M.; Wu, X.; Kollman, P. A. *AMBR 14*, University of Caifornia, San Franciso, 2014.
15. Koch, W.; Holthausen, M. C., *A Chemist's Guide to Density Functional Theory*. 2 ed.; Wiley-VCH Verlag GmbH: Weinheim 2001.

16. Frisch, M. J.; Trucks, G. W.; Schlegel, H. B.; Scuseria, G. E.; Robb, M. A.; Cheeseman, J. R.; Scalmani, G.; Barone, V.; Petersson, G. A.; Nakatsuji, H.; Li, X.; Caricato, M.; Marenich, A. V.; Bloino, J.; Janesko, B. G.; Gomperts, R.; Mennucci, B.; Hratchian, H. P.; Ortiz, J. V.; Izmaylov, A. F.; Sonnenberg, J. L.; Williams-Young, D.; Ding, F.; Lipparini, F.; Egidi, F.; Goings, J.; Peng, B.; Petrone, A.; Henderson, T.; Ranasinghe, D.; Zakrzewski, V. G.; Gao, J.; Rega, N.; Zheng, G.; Liang, W.; Hada, M.; Ehara, M.; Toyota, K.; Fukuda, R.; Hasegawa, J.; Ishida, M.; Nakajima, T.; Honda, Y.; Kitao, O.; Nakai, H.; Vreven, T.; Throssell, K.; J. A. Montgomery, J.; Peralta, J. E.; Ogliaro, F.; Bearpark, M. J.; Heyd, J. J.; Brothers, E. N.; Kudin, K. N.; Staroverov, V. N.; Keith, T. A.; Kobayashi, R.; Normand, J.; Raghavachari, K.; Rendell, A. P.; Burant, J. C.; Iyengar, S. S.; Tomasi, J.; Cossi, M.; Millam, J. M.; Klene, M.; Adamo, C.; Cammi, R.; Ochterski, J. W.; Martin, R. L.; Morokuma, K.; Farkas, O.; Foresman, J. B.; Fox, D. J. *Gaussian16, Revision A.03*, Gaussian, Inc.: Wallingford, CT, 2016.
17. Hay, P. J.; Wadt, W. R., Ab initio effective core potentials for molecular calculations – potentials for K to Au including the outermost core orbitals. *J. Chem. Phys.,* **1985,** *82*, 299-310.
18. Hehre, W. J.; Ditchfield, R.; Pople, J. A., Self—Consistent Molecular Orbital Methods. XII. Further Extensions of Gaussian—Type Basis Sets for Use in Molecular Orbital Studies of Organic Molecules. *J. Chem. Phys.* **1972,** *56*, 2257-2261.
19. Adamo, C.; Barone, V., Toward reliable density functional methods without adjustable parameters: The PBE0 model. *J. Chem. Phys.* **1999,** *110*, 6158-6170.
20. Adamo, C.; Scuseria, G. E.; Barone, V., Accurate excitation energies from time-dependent density functionl theory: Assessing the PBE0 model. *J. Chem. Phys.* **1999,** *111*, 2889-2899.
21. Grimme, S.; Antony, J.; Ehrlich, S.; Krieg, H., A consistent and accurate ab initio parametrization of density functional dispersion correction (DFT-D) for the 94 elements H-Pu. *J. Chem. Phys.* **2010,** *132*, 154104.
22. Berendsen, H. J. C.; Grigera, J. R.; Straatsma, T. P., The Missing Term in Effective Pair Potentials. *J. Phys. Chem.* **1987,** *91*, 6269-6271.
23. Heyda, J.; Pokorna, J.; Vrbka, L.; Vacha, R.; Jagoda-Cwiklik, B.; Konvalinka, J.; Jungwirth, P.; Vondrasek, J., Ion Specific Effects of Sodium and Potassium on the Catalytic Activity of HIV-1 Protease. *Phys. Chem. Chem. Phys.* **2009,** *11*, 7599−7604.
24. Isborn, C. M.; Gotz, A. W.; Clark, M. A.; R. C. Walker; Martinez, T. J., Electronic Absorption Spectra from MM and ab initio QM/MM Molecular Dynamics: Environmental Effects on the Absorption Spectrum of Photoactive Yellow Protein. *J. Chem. Theory Comput.* **2012,** *8*, 5092-5106.
25. Cossi, M.; Barone, V.; Cammi, R.; Tomasi, J., Ab initio study of solvated molecules: A new implementation of the polarizable continuum model. *Chem. Phys. Lett.* **1996,** *255*, 327-335.
26. Walker, R. C.; Crowley, M. F.; Case, D. A., The implementation of a fast and accurate QM/MM potential method in Amber. *J. Comput. Chem.* **2008,** *29*, 1019-1031.
27. Ryckaert, J. P.; Ciccotti, G.; Berendsen, H. J. C., Numerical-Integration of Cartesian Equations of Motion of a System with Constraints - Molecular-Dynamics of N-Alkanes. *J. Comput. Phys.* **1977,** *23*, 327−341.
28. Hornak, V.; Abel, R.; Okur, A.; Strockbine, B.; Roitberg, A.; Simmerling, C., Comparison of multiple Amber force fields and development of improved protein backbone parameters. *Proteins* **2006,** *65*, 712–725.
29. Cascella, M.; Magistrato, A.; Tavernelli, I.; Carloni, P.; Rothlisberger, U., Role of protein frame and solvent for the redox properties of azurin from Pseudomonas aeruginosa. *Proc. Natl. Acad. Sci. U.S.A.* **2006,** *52*, 19641–19646.